Global vector field reconstruction from a chaotic experimental signal in copper electrodissolution

C. Letellier, L. Le Sceller, E. Maréchal, P. Dutertre, B. Maheu, and G. Gouesbet
Laboratoire d'Energétique des Systèmes et Procédés, URA CNRS 230,
Institut National des Sciences Appliquées de Rouen, Boîte Postale 08, 76 131 Mont-Saint-Aignan, France

Z. Fei and J. L. Hudson
Department of Chemical Engineering, University of Virginia, Charlottesville, Virginia 22903
(Received 11 July 1994)

A successful global vector field reconstruction from experimental data that exhibit a chaotic behavior is obtained. Data arise from a copper electrodissolution. The reconstructed set of equations is checked by using a topological characterization.

PACS number(s): 05.45.+b, 87.40.+w

I. INTRODUCTION

Over the past few years many papers have been devoted to global vector field reconstruction [1–16]. In particular, the extraction of a set of equations that models the experimental data is a very important goal in the study of nonlinear systems. Such a model may allow a precise prediction of the evolution of the studied experimental system. If a good equivalence between the original attractor and the reconstructed attractor is achieved (for helpful discussion about this problem, see [17]), information on the evolution of the unobserved coupled variables required for the complete description of the system may then be available. Many developments on global reconstruction methods have been proposed essentially from numerical models, such as the well-known systems proposed by Lorenz [18] and Rössler [19].

In this paper, we present a successful reconstruction of an equation set from experimental chaotic data using derivative coordinates. With similar method, reconstructed models from experimental data have been obtained in Ref. [15]. The chaotic data studied here are obtained from the electrodissolution of copper [20]. Earlier data from the same system have been analyzed both by a discrete method as well as with a global vector field reconstruction using a continuous-time modeling with artificial neural networks [21,13]. A topological validation of the reconstructed model is given by extracting its template, which is found to be the same as the template of the experimental data. A similar use of a topological validation is also available from Tufillaro *et al.* [16].

The paper is organized as follows. Section II is devoted to a brief recall of the reconstruction method. Section III presents the experimental conditions and the extraction of the template from experimental data. In Sec. IV, the reconstructed model is given and its template is built and favorably compared to the original one. Section V gives a conclusion.

II. RECONSTRUCTION METHOD

For a more convenient presentation, we present the reconstruction method in the case where the required number of equations is equal to 3. The aim of such a method is to reconstruct a vector field equivalent to the original system from a scalar time series, here called $x(t)$. A standard system can be written with the observable $x(t)$ and its derivatives according to

$$\dot{X} = \dot{x} = Y, \quad \dot{Y} = Z, \quad \dot{Z} = F(X, Y, Z) \ , \tag{1}$$

in which the reconstructed state space related to the standard system is spanned by derivative coordinates $(X = x, Y = \dot{x}, Z = \ddot{x})$.

A global vector field reconstruction may then be achieved if a good enough approximation $\tilde{F}$ of the so-called standard function F is designed. The approximation $\tilde{F}$ is obtained by using a Fourier expansion on a basis of orthonormal multivariate polynomials generated by the data set [14,7]. These polynomials depend on the derivative coordinates (X, Y, Z), therefore involving terms X^i, Y^j, Z^k. As described in Ref. [14], we introduce monomials P^l which read

$$P^l = X^i Y^j Z^k \ . \tag{2}$$

The one-to-one relationship to be used between triplets (i, j, k) and natural numbers l is completely defined in [14]. The approximation of the function F may then be written as

$$\tilde{F} = \sum_{l=1}^{N_l} K_l \, P^l \ , \tag{3}$$

where N_l is the dimension of the basis $\{P^l\}$. All the information concerning the chaotic attractor is therefore encoded in the set of coefficients K_l, which forms a sig-

nature of the attractor.

The time derivatives used in this algorithm are estimated by a discrete linear filter

$$w_j(t) = \sum_{n=-p}^{p} r_{j,p}(n)\, x(t+n\tau)\ , \tag{4}$$

where the time series $x(t)$ discretized on the time step τ is the input, $w_j(t)$, the so-called Legendre coordinate, is the output, and $r_{j,p}(n)$ is an appropriate discrete convolution kernel, namely, the discrete Legendre polynomials, parametrized by the choice of p and the order j of the required derivative. Following Gibson *et al.* [22], this filter defines the optimal linear coordinate transformation.

It appears [14] that the reconstruction depends on N_q, the number of vectors $(x, \dot{x}, \ddot{x}, \dddot{x})$ on which F is estimated; N_s, the number of vectors sampled per pseudo-period; N_l, the number of retained multivariate polynomials; and $\tau_w = (2p+1)\tau$, the window size on which the derivatives are estimated by using the linear filter (4). The vector $(\tau, N_q, N_s, N_l, \tau_w)$ defines all the reconstruction parameters. In practical applications, the choice of such parameters may have a significant effect on the quality of the results [14]. Optimal parameters may be more easily obtained by using an error function E_r given by (in shorthand notation)

$$E_r = \frac{\|\dot{Z} - \tilde{F}(X,Y,Z)\|_1}{\|\dot{Z}\|_1}\ , \tag{5}$$

where $\|\ \|_1$ is a norm chosen to be the norm L_1 due to its computational efficiency. The use of such an error function is similar to the one introduced by Brown *et al.* [15].

III. COPPER ELECTRODISSOLUTION

It is well established that chemical reactions may provide chaotic behaviors, for instance, the Belousov-Zhabotinskii reaction ([23–26]) and many electrodissolutions [27,28]. We investigate here the case of a copper electrodissolution.

A. Experiments

The time series was obtained from a dissolution current measurement during the potentiostatic electrodissolution of a rotating Cu electrode in phosphoric acid. The experimental setup consisted of a rotating disk electrode, which had a copper rod, 8.26 mm in diameter, embedded in a 2-cm-diam Teflon cylinder. The rotating speed was maintained at 4400 rpm. In order to minimize noise, we used a mercury contact instead of standard silver-carbon brush contact (Pine Instrument ASR2 rotator). A cylindrical platinum net band (much larger than the disk) was put around the disk as a counter electrode to get uniform potential and current distributions.

The cell was a 500-ml flask with a side neck in which the capillary probe was fixed. The reference electrode

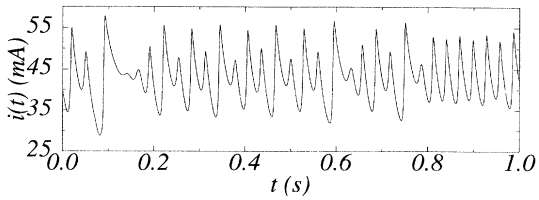

FIG. 1. Current times series $I(t)$.

was a saturated calomel electrode (SCE), which was separated from the solution by the capillary. The distance between the disk surface and the tip of the capillary was about 6 mm. The cell contained 250 ml of 85.7 wt. % phosphoric acid and a water bath was used to maintain its temperature at 20 °C.

A Potentiostat (Princeton Applied Research model 273) was used to regulate the potential (at 689 mV) of the working disk electrode with respect to the SCE and to monitor the current. The data were recorded at a frequency of $f_e = 1500$ Hz using a 486-type personal computer and a data acquisition board (Model DAS-16, Keithley MetraByte's). The current time series $I(t)$ is displayed in Fig. 1.

Once the initial transient signal has disappeared, the behavior of the system eventually settles down on a chaotic attractor in the state space. Such a space may be reconstructed by using derivative coordinates (X, Y, Z) as proposed in the pioneering paper by Packard *et al.* [1]. Since we find a correlation dimension D_2 equal to 2.3 ± 0.2 by using the Grassberger-Proccacia algorithm [29], the reconstructed standard space may be spanned by using three coordinates as displayed in Fig. 2.

A first-return map to the Poincaré section P is defined by

$$P \equiv \{(X,Y) \in I\!R^2 \mid X = 43.7,\ Y > 0\} \tag{6}$$

and displayed in Fig. 3. Two monotonic branches are distinguished: one increasing branch and one decreasing branch, which allow us to define a symbolic dynamics to encode periodic orbits.

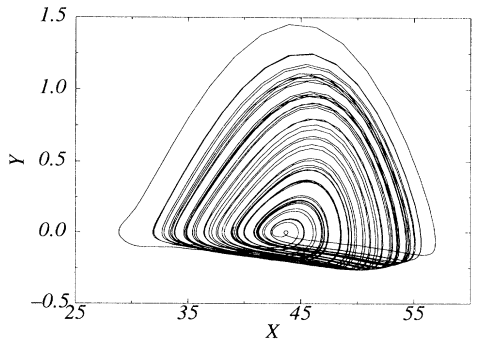

FIG. 2. XY-plane projection of the reconstructed state space. Derivatives are estimated by using the discrete Legendre filter with a window size $\tau_w = 21 f_e^{-1}$.

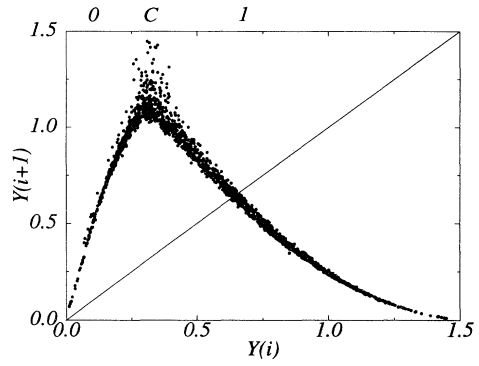

FIG. 3. First-return map to the Poincaré section P.

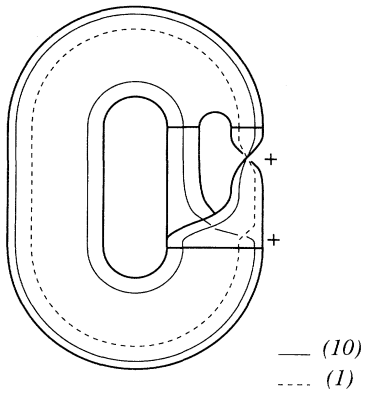

FIG. 4. Template of the original attractor. The orbit pair (1,10) is constructed: $L(1,10) = \frac{1}{2}[+2] = +1$.

B. Template

Topological characterization provides a useful tool to decide about the equivalence between an original attractor (here obtained by a reconstruction in the space spanned by the derivative coordinates, displayed in Fig. 2) and a reconstructed attractor (here generated by integrating the reconstructed vector field, displayed in Fig. 7). The first step is then the construction of the template from experimental data. For that purpose the usual procedure [30] is to propose an induced template and check it by a comparison between linking numbers obtained from orbit constructions on the template and plane projections of the corresponding orbits (extracted from the experimental data): if the linking numbers are found to be equal, the template is checked.

The attractor displayed in Fig. 2 is a very simply folded band like the common Rössler attractor. From the first-return map, we propose a template consisting of two stripes: one stripe without any local torsion associated with branch 0 and one stripe with a positive π twist (following the convention introduced by Melvin and Tufillaro [31]) associated with branch 1. Such a process does

TABLE I. Values of K_l.

l	K_l	l	K_l
1	0.1219705394981005	27	−0.145539951745097
2	$-1.078249529843902 \times 10^{-2}$	28	0.1049018763188871
3	0.9125082050943352	29	12.14985173080021
4	−31.5804652088144	30	−38.5366235437547
5	$2.882119184023051 \times 10^{-4}$	31	0.3809613670493999
6	−0.107945627123624	32	2.19570526400687
7	3.14261019012943	33	21.55254081698994
8	−2.58142102535676	34	165.1484278847694
9	30.7789877436226	35	−1437.72802782965
10	180.3217927930279	36	$7.928626337606531 \times 10^{-10}$
11	$-5.550910841337609 \times 10^{-7}$	37	$5.752046655223851 \times 10^{-7}$
12	$4.625376454207544 \times 10^{-3}$	38	$-1.081602890433014 \times 10^{-5}$
13	−0.114822275266309	39	$4.628712833151052 \times 10^{-5}$
14	0.2121650714651616	40	$-3.976058731703460 \times 10^{-4}$
15	−2.24124505814176	41	$-2.626758361863347 \times 10^{-3}$
16	−13.6799701248913	42	$1.437994615429103 \times 10^{-3}$
17	3.60656873135868	43	$1.753989520753347 \times 10^{-4}$
18	−6.67239615224999	44	−0.126567212485869
19	−287.70105676069	45	0.3435285584041194
20	1083.030601671941	46	$-5.116362209078044 \times 10^{-3}$
21	$-7.711227398599053 \times 10^{-8}$	47	$-3.788259242947936 \times 10^{-2}$
22	$-8.541800526483852 \times 10^{-5}$	48	−0.572245746550728
23	$1.833011097559745 \times 10^{-3}$	49	−4.44596569136184
24	$-5.532917786559483 \times 10^{-3}$	50	23.99099286766239
25	$5.276461759803514 \times 10^{-2}$	51	$-8.936897340164367 \times 10^{-2}$
26	0.3345112248727262	52	−0.464973703176679

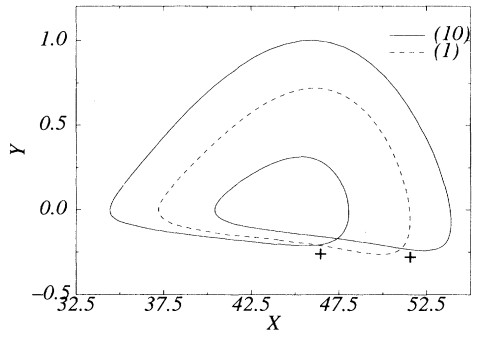

FIG. 5. Projection of the orbit couple (1,10) on the XY plane: $L(1,10) = \frac{1}{2}[+2] = +1$.

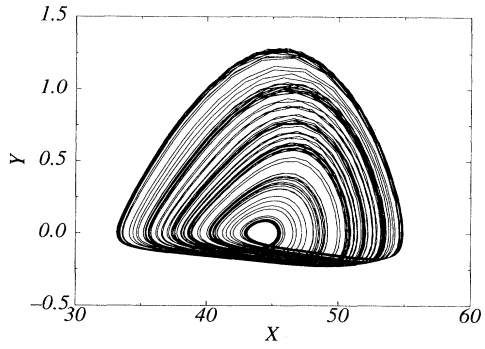

FIG. 7. Reconstructed attractor generated by integrating the reconstructed model.

not allow us to identify global torsions in the template, which therefore will have to be validated.

The template is displayed in Fig. 4 together with a pair of periodic orbits encoded by (1) and (10), respectively. The linking number $L(1,10)$, which is equal to the half sum of oriented crossings [31,32], turns out to be equal to $+1$.

In order to check this template, the XY-plane projections of a few orbit couples are required. Periodic orbits (1), (10), and (1011) are extracted by a close return method from the time series $I(t)$ and are projected on the XY planes (Figs. 5 and 6). The half sum of oriented crossings of the pair (1,10) is found to be equal to $+1$ as on the template. The second linking number $L(10,1011)$ is also counted on the XY plane and is found to be equal to $+3$ (which may be easily checked on the template). The template is therefore checked.

IV. RECONSTRUCTED MODEL

A. Model

A reconstructed model is obtained by applying the algorithm previously described in Sec. II. Required suc-

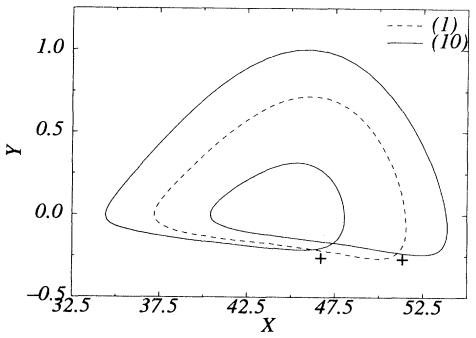

FIG. 8. X plane projection of periodic orbits encoded by (1) and (10), respectively. $L(1,10) = \frac{1}{2}[+2] = +1$.

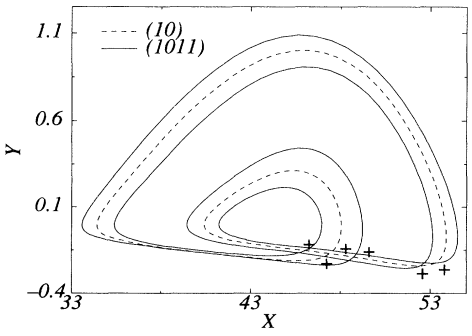

FIG. 6. Projection of the orbit couple (10,1011) on the XY plane: $L(10,1011) = \frac{1}{2}[+6] = +3$.

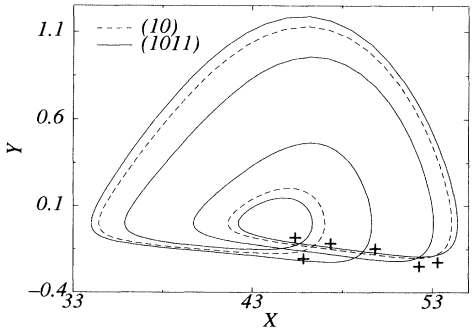

FIG. 9. XY plane projection of periodic orbits encoded by (10) and (1011), respectively. $L(10,1011) = \frac{1}{2}[+6] = +3$.

cessive derivatives of the time series $I(t)$ are estimated by using the discrete Legendre filter with a window size $\tau_w = 21 f_e^{-1} \approx 0.015$. The central little loop in Fig. 2 is not considered to be representative of the dynamical behavior. Thus we choose a part of data without any loop to perform our algorithm. After searching the minimal value of the error function E_r, it is found that an optimal reconstruction vector is $(\tau, N_q, N_s, N_l, \tau_w) = (f_e^{-1}, 295, 14, 52, 21 f_e^{-1})$, i.e., a successful reconstruction is obtained with an approximate standard function $\tilde{F}$ of 52 terms. K_l values are reported in Table I.

The reconstructed standard system is then integrated with an adaptative step integrator. The reconstructed attractor is displayed in Fig. 7, comparing rather well with Fig. 2.

B. Topological equivalence validation

In order to validate this model, a template is built from the attractor generated by the integration of the model. Periodic orbits are extracted and projected on the XY plane (Figs. 8 and 9). Linking numbers $L(1, 10)$ and $L(10, 1011)$ are equal to $+1$ and $+3$ as on the original attractor, respectively. The model is therefore topologically compatible with the experimental data.

V. CONCLUSION

We presented a global vector field reconstruction of an experimental chaotic data set in the case of copper electrodissolution. The obtained model is checked by topological characterization, which gives identical templates for the attractor reconstructed with successive derivatives and the attractor generated by integrating the reconstructed model. Such a model may be used to predict the evolution of the observable and also of unobserved variables. A very accurate study of the population of periodic orbits related to these attractors (original and reconstructed ones) will be presented in a future paper. With such results, it is believed that physicists now possess an opportunity to extract automatic models from experimental time series and to exploit them.

ACKNOWLEDGMENT

Grateful acknowledgement is made to the National Science Foundation for partial support of this work.

[1] N. H. Packard, J. P. Crutchfield, J. D. Farmer, and R. S. Shaw, Phys. Rev. Lett. **45**, 712 (1980).
[2] J. P. Crutchfield and B. S. McNamara, Complex Syst. **1**, 417 (1987).
[3] J. D. Farmer and J. J. Sidorowitch, Phys. Rev. Lett. **59**, 845 (1987).
[4] A. K. Agarwal, D. P. Ahalpara, P. K. Kaw, H. R. Prablakera, and A. Sen, J. Phys. **35**, 287 (1990).
[5] J. L. Breeden and A. Hübler, Phys. Rev. A **42**, 5817 (1990).
[6] M. Casdagli, S. Eubank, J. D. Farmer, and J. Gibson, Physica D **51**, 52 (1991).
[7] M. Giona, F. Lendini, and V. Cimagalli, Phys. Rev. A **44**, 3496 (1991).
[8] G. Gouesbet, Phys. Rev. A **43**, 5321 (1991).
[9] G. Gouesbet, Phys. Rev. A **44**, 6264 (1991).
[10] M. Palus and I. Dvoràck, Physica D **55**, 221 (1992).
[11] G. Gouesbet, Phys. Rev. A **46**, 1784 (1992).
[12] G. Gouesbet and J. Maquet, Physica D **58**, 202 (1992).
[13] R. Rico-Martinez, K. Krischer, I. G. Kevrekidis, M. Kube, and J. L. Hudson, Chem. Eng. Commun. **118**, 25 (1992).
[14] G. Gouesbet and C. Letellier, Phys. Rev. E **49**, 4955 (1994).
[15] R. Brown, N. F. Rulkov, and E. R. Tracy, Phys. Rev. E **49**, 3784 (1994).
[16] N. B. Tufillaro, P. Wyckoff, R. Brown, T. Schreiber, and T. Molteno, Phys. Rev. E **51**, 164 (1995).
[17] C. Letellier and G. Gouesbet (unpublished).
[18] E. N. Lorenz, J. Atmos. Sci. **20**, 130 (1963).
[19] O. E. Rössler, Phys. Lett. **57A**, 397 (1976).
[20] J. L. Hudson and T. T. Tsotsis, Chem. Eng. Sci. **49**, 1493 (1994).
[21] J. L. Hudson, M. Kube, R. A. Adomaitis, I. G. Kevrekidis, A. S. Lapedes, and R. M. Farber, Chem. Eng. Sci. **45**, 2075 (1990).
[22] J. F. Gibson, J. D. Farmer, M. Casdagli, and S. Eubank, Physica D **57**, 1 (1992).
[23] J. L. Hudson, M. Hart, and D. Marinko, J. Chem. Phys. **71**, 1601 (1979).
[24] J. C. Roux, A. Rossi, S. Bachelart, and C. Vidal, Phys. Lett. **77A**, 391 (1980).
[25] J. L. Hudson, Z. Phys. Chem. **270**, 497 (1989).
[26] A. Arnéodo, F. Argoul, J. Elezgaray, and P. Richetti, Physica D **62**, 134 (1993).
[27] M. R. Bassett and J. L. Hudson, J. Phys. Chem. **93**, 2731 (1989).
[28] M. R. Bassett and J. L. Hudson, J. Electrochemical Society **137**, 1815 (1990).
[29] P. Grassberger and I. Proccacia, Physica D **9**, 189 (1983).
[30] G. B. Mindlin, H. G. Solari, M. A. Natiello, R. Gilmore, and X. J. Hou, J. Nonlin. Sci. **1**, 147 (1991).
[31] P. Melvin and N. B. Tufillaro, Phys. Rev. A **44**, 3419 (1991).
[32] G. B. Mindlin, X. J. Hou, H. G. Solari, R. Gilmore, and N. B. Tufillaro, Phys. Rev. Lett. **64**, 2350 (1990).